

Article

High-Resolution Measurement of Molecular Internal Polarization Structure by Photoinduced Force Microscopy

Hidemasa Yamane ^{1,†} , Nobuhiko Yokoshi ¹  and Hajime Ishihara ^{1,2,3,*} 

¹ Department of Physics and Electronics, Osaka Prefecture University, 1-1 Gakuen-cho, Naka-ku, Sakai, Osaka 599-8531, Japan; h.yamane@kitasato-u.ac.jp (H.Y.); yokoshi@pe.osakafu-u.ac.jp (N.Y.)

² Department of Materials Engineering Science, Osaka University, 1-3 Machikaneyama-cho, Toyonaka, Osaka 560-8531, Japan

³ Center for Quantum Information and Quantum Biology, Osaka University, 1-1 Yamadaoka, Suita, Osaka 565-0871, Japan

* Correspondence: ishi@mp.es.osaka-u.ac.jp

† Current address: Department of Physics, Kitasato University, 1-15-1 Kitazato, Minami-ku, Sagami-hara, Kanagawa 252-0373, Japan.

Abstract: Near-field interactions between metallic surfaces and single molecules play an essential role in the application of metamaterials. To reveal the near-field around a photo-irradiated single molecule on the metallic surface, high-resolution photo-assisted scanning microscopy is required. In this study, we theoretically propose photoinduced force microscopy (PiFM) measurements of single molecules at the atomic resolution. For experimental demonstration, we performed a numerical calculation of PiFM images of various transition states, including optical forbidden transitions, and interpreted them in terms of the interaction between the molecular internal polarization structures and localized plasmon. We also clarified the critical role of atomic-scale structures on the tip surface for high-resolution PiFM measurements.

Keywords: photoinduced force microscopy; localized plasmons; optical forbidden transition



Citation: Yamane, H.; Yokoshi, N.; Ishihara, H. High-Resolution Measurement of Molecular Internal Polarization Structure by Photoinduced Force Microscopy. *Appl. Sci.* **2021**, *11*, 6937. <https://doi.org/10.3390/app11156937>

Academic Editor: Edik U. Rafailov and Tatjana Gric

Received: 30 June 2021

Accepted: 26 July 2021

Published: 28 July 2021

Publisher's Note: MDPI stays neutral with regard to jurisdictional claims in published maps and institutional affiliations.



Copyright: © 2021 by the authors. Licensee MDPI, Basel, Switzerland. This article is an open access article distributed under the terms and conditions of the Creative Commons Attribution (CC BY) license (<https://creativecommons.org/licenses/by/4.0/>).

1. Introduction

A fascinating feature of metamaterials is their ability to manipulate and enhance chiral fields, leading to peculiar interactions with chiral matter systems. Several metamaterial structures have been proposed and have demonstrated large circular dichroism (CD) [1–4]. Interestingly, the superchiral fields originated by such metamaterials boost the molecular CD signals and enable highly sensitive enantioselective detection of chiral molecules [5–8]. These results indicate that the elucidation of the interaction between metamaterials and molecular systems is an important factor for the future development of metamaterials for relevant applications. Although in [5–8], the authors have shown that near-field interactions of metallic surfaces and molecules should play an essential role in the above-mentioned metamaterial effects, it is still challenging to reveal the spatial structures of the near-field around a single molecule because of the limited resolution of existing photo-assisted microscopic techniques.

Photoinduced force microscopy (PiFM), which detects photoinduced force (gradient force) using atomic force microscopy, is a promising approach to address this problem [9,10]. To observe the optical response of single molecules, various types of scanning microscopic techniques have been developed, such as scanning tunneling microscopy luminescence (STML) [11,12], tip-enhanced Raman spectroscopy (TERS) [13,14], and the atomic force microscopy (AFM) with CO-terminated tip [15]. PiFM can be used as a complement to these microscopic techniques because unlike these methods, PiFM does not detect propagating light but directly obtains information of the localized near-field associated with molecules as the force. In particular, PiFM has the advantages of proving vertical polarization of the near-field, detection of buried objects, and no propagation loss [16–19]. Recently,

heterodyne frequency modulation, an innovative measurement technique that enables high-precision and high-resolution PiFM measurements to eliminate photothermal oscillations, has been developed [20,21]. Further development is expected for atomic resolution PiFM measurements of single molecules. By utilizing such properties of PiFM, we can elucidate the near-field interaction between metamaterials and single molecules. For this purpose, it is important to theoretically clarify how the intrinsic optical response of each molecule can be “seen” by PiFM.

Thus, in this study, we theoretically propose PiFM measurements for a single molecule with a size smaller than 1 nm. In the PiFM system, because the molecules strongly interact with the localized plasmon enhanced at the gap between the tip and substrate, the interaction between the total field created by the entire system, including the molecule, and the polarization of all materials, must be treated self-consistently. By using the discrete dipole approximation (DDA) method, we numerically analyzed the total response field in the PiFM measurements and evaluated the radiation force acting on the tip. We show PiFM images for molecular excitation, including the optical forbidden transition beyond the long-wavelength approximation, and provide an interpretation in terms of the microscopic interaction between the molecule and the localized plasmon. In particular, under the electronic resonance, experimentally obtained images of PiFM become complicated, and hence, the theoretical simulations will be useful for interpreting the images. We also investigated how atomic-scale structures on the tip surface, picocavity [22], play an important role in the atomic resolution measurement of PiFM, which detects the field gradient of localized plasmons.

2. Theory and Calculation Model

2.1. Discrete Dipole Approximation

We calculated the self-consistent total response electric field induced in a nanogap made of a tip, single molecule, and substrate by using the DDA method:

$$\mathbf{E}(\mathbf{r}_i, \omega) = \mathbf{E}_0(\mathbf{r}_i, \omega) + \sum_j V \mathbf{G}(\mathbf{r}_i, \mathbf{r}_j, \omega) \mathbf{P}(\mathbf{r}_j, \omega), \quad (1)$$

$$\mathbf{P}(\mathbf{r}_i, \omega) = \chi(\mathbf{r}_i, \omega) \mathbf{E}(\mathbf{r}_i, \omega), \quad (2)$$

where $\mathbf{E}(\mathbf{r}_i, \omega)$ and $\mathbf{E}_0(\mathbf{r}_i, \omega)$ represent the total response field and incident field, respectively; i is the index of cells at the coordinate \mathbf{r}_i ; and ω is the angular frequency of the electric field. $\mathbf{G}(\mathbf{r}_i, \mathbf{r}_j, \omega)$ is the free-space green function propagating in both the transverse and longitudinal electromagnetic fields. $\mathbf{P}(\mathbf{r}_j, \omega)$ is the polarization of the j -th cell, and the integral of the second term in Equation (1) represents the field at the i -th cell propagated from the polarization at the j -th cell. V is the volume of the unit cell. Polarization is described by local susceptibility $\chi(\mathbf{r}_i, \omega)$. In the DDA method, because the entire space must be divided into cells of the size necessary to describe microscopic structures, it is not realistic to perform calculations that consider the atomic-scale structures of the molecules and macroscopic PiFM system. To solve the problem of this computational size, we employed an extended DDA method that incorporates partial subdivision [23]. The photoinduced force acting on the tip was obtained as follows [24]:

$$\mathbf{F}(\omega) = \frac{1}{2} \text{Re} \left[\sum_i V (\nabla \mathbf{E}^*(\mathbf{r}_i, \omega)) \cdot \mathbf{P}(\mathbf{r}_i, \omega) \right], \quad (3)$$

where the summation is performed on the cells that configure the tip.

2.2. Model Parameters

We assumed that the tip is made of gold and the substrate is a gold film. The metallic structures are assumed to have a Drude-type susceptibility with the parameters of Au

$$\chi_{\text{Au}}(\omega) = \frac{1}{4\pi} \left[\epsilon_{\text{Au}} - \epsilon_0 - \frac{(\hbar\omega_{\text{Au}})^2}{(\hbar\omega)^2 + i\hbar\omega \left(\gamma_{\text{bulk}} + \frac{\hbar V_{\text{F}}}{L_{\text{eff}}} \right)} \right], \quad (4)$$

where ϵ_{Au} is the background dielectric constant of the metal; ϵ_0 is the dielectric constant of vacuum; ω_{Au} is the bulk plasma frequency; γ_{bulk} is the electron relaxation constant of bulk gold; V_{F} is the electron velocity at the Fermi level; and L_{eff} is the effective mean free path of electrons, which is comparable to the size of the tip diameter. The following parameters were used for the gold structures: $\epsilon_{\text{Au}} = 12.0$, $\epsilon_0 = 1.0$, $\hbar\omega_{\text{Au}} = 8.958$ eV, $\gamma_{\text{bulk}} = 72.3$ meV, $\hbar V_{\text{F}} = 0.922$ nm · eV, and $L_{\text{eff}} = 60$ nm [25,26].

3. PiFM Measurement for a Single-Molecule

We demonstrate PiFM measurements of a single molecule using a simplified model to understand the microscopic interaction between the molecule and the localized plasmon. We consider a PiFM system and six-membered ring molecule by DDA with a discretized unit cell size of 1 Å, as shown in Figure 1a,b. In the present study, we put stress on discussing the relationship between the geometrical structure of a molecule and the PiFM image having spatial structures inside the single molecule. That is why we use the simplified model of a molecule. The results obtained by using the orbital functions of a more realistic model will be published elsewhere. The tip is assumed to be a 60 nm diameter gold sphere with several protrusions, forming picocavity, on the apex, which is known in the field of tip-enhanced Raman spectroscopy [14,22]. The substrate is assumed to be a gold thin film with a thickness of 9 nm. The susceptibility of the metallic substrate is given by the Drude model with the parameter of Au, and each of the six elements of the molecule are determined by the Lorentz model as follows:

$$\chi_{\text{np}}(\omega) = \frac{1}{4\pi} \left[\epsilon_{\text{np}} - \epsilon_0 - \frac{|\mu|^2/V_{\text{np}}}{\hbar\omega_{\text{np}} - \hbar\omega - i\gamma_{\text{np}}} \right], \quad (5)$$

where ϵ_{np} , μ , V_{np} , $\hbar\omega_{\text{np}}$, and γ_{np} are the background dielectric constant, dipole moment, volume, resonant energy, and damping constant of the elements of the six-membered ring molecule, respectively. For simplicity, we considered that the polarization is restricted in the molecular plane and the susceptibility is local. We assume elements with resonant energies of $\hbar\omega_{\text{np}} = 2.0$, and the dipole moment of 1 Debye, which is similar to the value for porphyrin-based dye molecules [18,27,28], with parameters $\epsilon_{\text{np}} = 1.5$, $\gamma_{\text{np}} = 5$ meV, and $V_{\text{np}} = 1$ Å³, which is the same as the unit cell V . We assume a gap of 3 Å between the molecule and substrate, considering the experimental situation. A few atomic layers of a dielectric, such as NaCl, are laid down as spacers to avoid hybridization between the molecular orbitals of the sample and the metal substrate in the measurement of molecules, such as STM [11,12].

The six dipoles of the molecule can take on various spatial structures, each of which has a specific resonance state. Figure 1c,d show the absorption cross-section spectrum in a vacuum and the polarization structures of the molecule for each resonant energy, respectively. These peaks correspond to optical allowed transitions under the long-wavelength approximation.

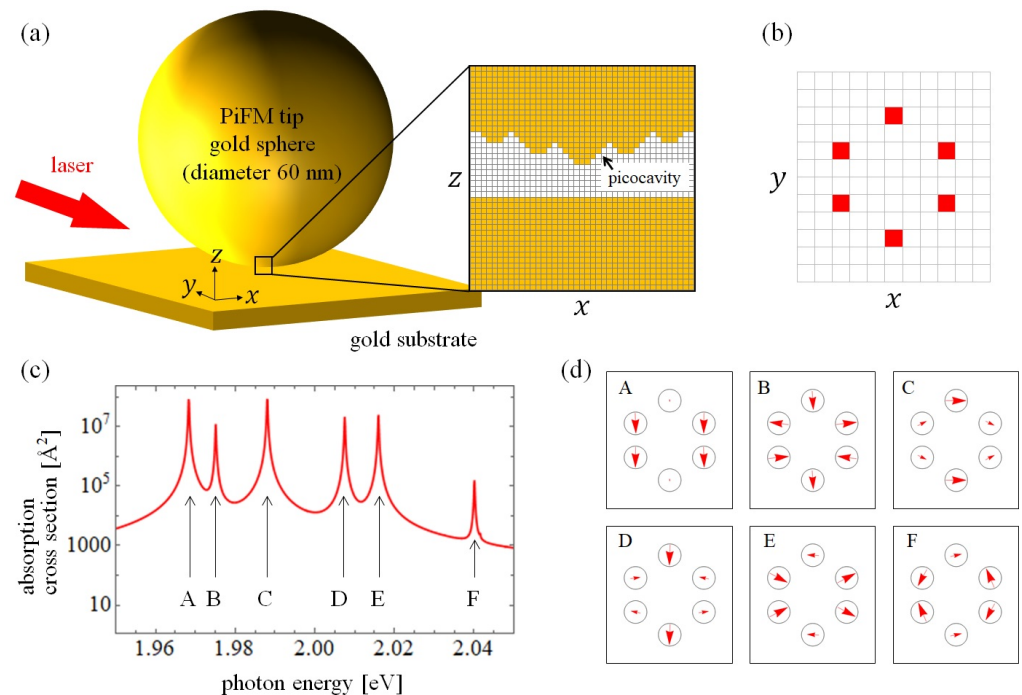


Figure 1. (a) Schematic PiFM model. The tip has atomic-scale structures, which form a picocavity on its apex. (b) Simplified model of a six-membered ring molecule on the substrate. The susceptibility of each element of the molecule was defined using the Lorentz model. The entire space was discretized into 1 \AA^3 cubic cells represented by grid lines. (c) Absorption spectrum of a six-membered ring molecule in vacuum. The peaks correspond to the resonance states under long-wavelength approximation. (d) The spatial structures of the dipoles in the molecule at each resonance energy, as shown in (c).

3.1. Microscopic Interaction between Molecule and Plasmon

We discuss the PiFM (attractive force) spectra for the molecule, which are shown in Figure 2 as solid colored lines when the PiFM tip placed at each position. The dashed line represents the spectrum of the gold substrate, that is, in the absence of the molecule. The PiFM spectra show that PiFM has a high sensitivity for the wavelength of the incident laser, and different resonance states can be observed depending on the position of the tip, resulting in a high spatial resolution. This is due to the significant localization and enhancement of localized surface plasmons by the atomic-level spatial structure called picocavity at the tip apex [22]. In addition, a Fano-like structure with an asymmetric peak-dip structure appears near the molecular resonance energy in the PiFM spectrum. This can be caused by the interference effect between the broad plasmon resonance peak and the sharp molecular resonance peak, which has been explained in our previous work [18]. When light with energy lower than the resonance energy of the molecule is incident, the polarization of the plasmon and the polarization of the molecule are in phase. As these enhance each other, the photoinduced force is clearly observed in the direction of attraction. In contrast, when light with an energy higher than the resonance energy of the molecule is incident, the polarization of the molecule and the plasmon are in anti-phase, and they suppress each other. In this case, the polarization of the molecule was very small and only slightly weakened the plasmon. Therefore, the peak in the attraction direction was large, and the dip in the repulsion direction was small.

We calculated the PiFM images and polarization structures at each peak of the PiFM spectrum shown in Figure 2. As shown in Figure 3a–e, completely different PiFM images were obtained for each resonance energy of the molecule. The calculated spatial polarization structures for the respective PiFM images are shown in Figure 3f–j. Figure 3f,g are optically allowed transitions that can be excited under the long-wavelength approximation,

whereas Figure 3h–j are forbidden transitions, where the average of the polarization inside the molecule vanishes. The difference between these PiFM images can be understood by the interaction with the electric field vector of the plasmon spreading isotropically from the tip apex. The features of these images agree with the discussion of a previous study on molecular imaging by TERS [13].

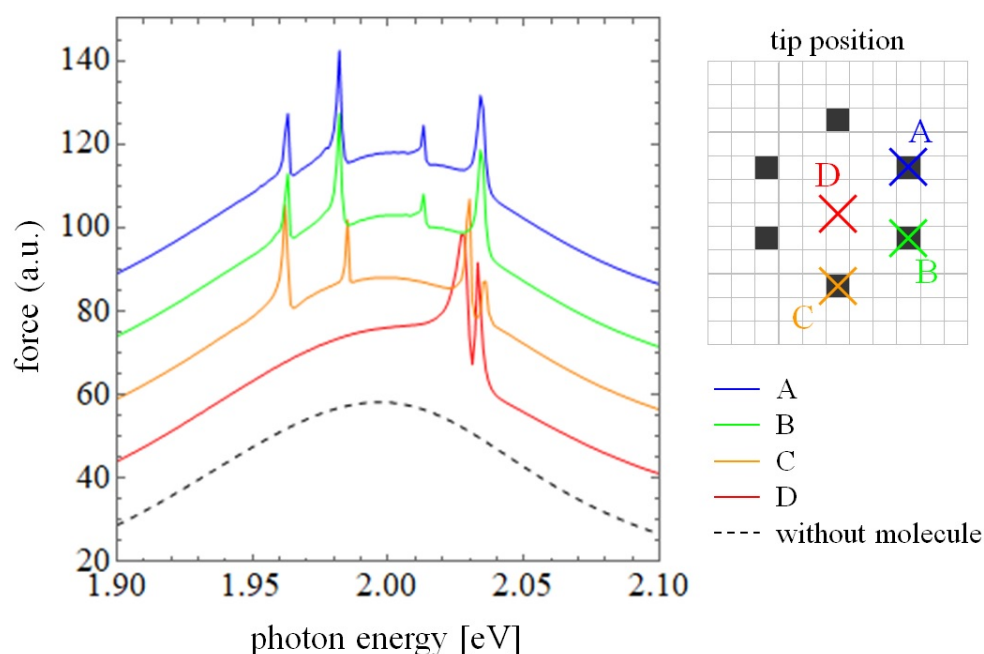


Figure 2. Photoinduced force spectra of the six-membered molecule. The solid lines are the force spectra for the respective tip positions, and the dashed line represents the force spectrum for the tip on the substrate, that is, in the absence of the molecule.

In the allowed transition, shown in Figure 3a,b, when the tip is at the center of the molecule, two robe-like PiFM images and the nodes are observed. Because the electric field vectors of the localized plasmon spread radially around the tip apex, when the polarizations of plasmons and molecules are in the same line, the molecule is excited and the force signal is obtained, as shown in Figure 4a. In contrast, when the polarizations of plasmons and molecules are orthogonal, the molecule cannot be excited, and the node appears in the PiFM image, as shown in Figure 4b.

For optically forbidden transitions, the molecule can be excited when the tip is at a position where the dipoles are opposed to each other, as shown in Figure 4c. In Figure 3c, when the tip is at the center of the molecule, the dipoles of the two diagonal elements in the y -axis direction are in phase with the plasmon but the other four elements are in the opposite phase; therefore, they cancel each other out and the molecule cannot be excited. In contrast, in Figure 3d, when the tip is at the center of the molecule, all dipoles of the molecule are in phase with the plasmon, so the PiFM image appears at the center of the molecule. In Figure 3e, the structure of the dipoles is similar to Figure 3d, but when the tip is at the center of the molecule, the four dipoles on the sides from the y -axis are orthogonal with the plasmon; thus, the PiFM image is a little weaker at the center and shows a torus-like structure.

In this section, although we analyzed the PiFM measurements of a simple model that mimics a six-membered ring molecule, we obtained a qualitative understanding from the perspective of the interaction between the polarization structure inside the molecule and the localized plasmon. The results we obtained facilitate the understanding of PiFM measurements in a realistic analysis and experiments.

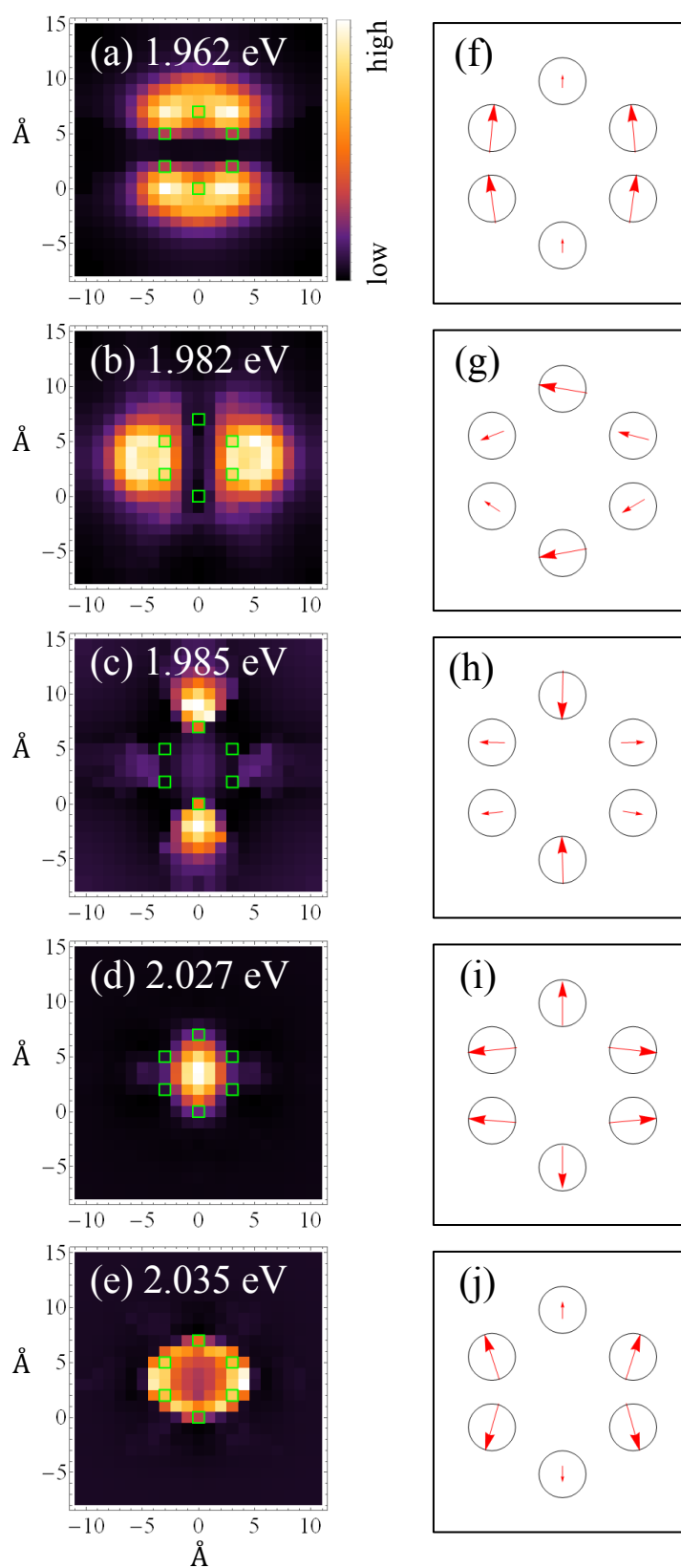


Figure 3. (a–e) are PiFM images for the resonance states. The green squares represent the positions of each element of the six-membered molecule. (f–j) represent the dipole structures of the molecule corresponding to the PiFM image above. The circles represent the elements of the six-membered molecule, and the red arrows represent the polarization vectors.

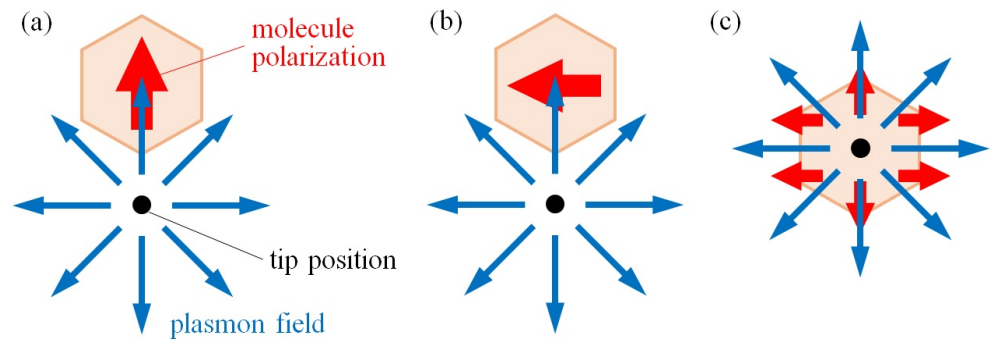


Figure 4. Excitable conditions of a molecule by plasmon (top view). The hexagon and red arrows represent the molecule and molecular polarization, respectively. The black dot represents the tip position and the blue arrows are the electric field vector of the localized plasmon induced at the tip-substrate nanogap. (a,b) show the excitable and non-excitable tip position conditions for the allowed transition of the molecule, as shown in Figure 3f,g, respectively. (c) shows the excitable tip position condition for a forbidden transition of the molecule, as shown in Figure 3j.

3.2. Critical Role of Picocavity in Resolution

In this section, we discuss the feasibility of atomic resolution measurements using PiFM. We revealed that the atomic structure on the tip surface, which has recently been called picocavity [22] in the field of TERS, plays an important role in PiFM resolution. We consider a tip model that imitates the gathering of atoms, as shown in Figure 5a,b. The alignment of the protrusions is not important for resolution. Rather, it is easier to consider only one protrusion in terms of resolution. Considering the atomic structure on the tip surface, it is necessary to consider whether ghost images caused by other protrusions can be avoided.

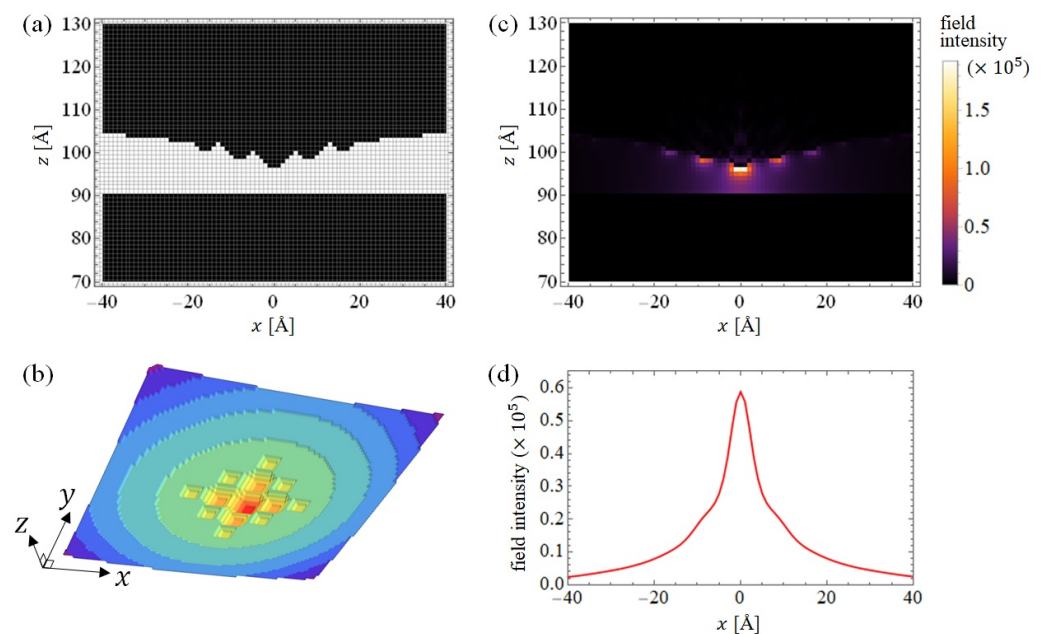


Figure 5. (a,b) show the model tip with picocavity in the cross-sectional picture of the tip center and the three-dimensional picture of the bottom view, respectively, in discretized space. The colors in (b) represent contour maps. (c) shows a map of the response field intensity from the viewpoint of (a). The intensity is determined as a ratio of the incident field, $|E|^2/|E_0|^2$. (d) is the line profile of the field intensity at 3 Å below the tip apex.

Figure 5c,d show the response field intensity map and line profile at the plane of 3 Å below from the tip apex, respectively, irradiated with the incident laser. The intensity was determined as a ratio to the incident field, $|E|^2/|E_0|^2$. The enhanced field is extremely localized in the vicinity of the picocavity. Naturally, the sharpness of the tip contributes to high-resolution imaging. However, in scanning optical microscopic techniques, such as TERS and PiFM, the enhancement and localization of the field are also determinant factors for high-resolution imaging. The force curve of the PiFM is steep [21], and the contribution from the other protrusions is negligible.

In our previous study, we experimentally and theoretically demonstrated that the nanometer-scale structure on the tip surface enabled us to realize a resolution of PiFM measurement of less than 1 nm at room temperature [19]. In this study, we considered a tip with picocavity; however, our study is based on the assumption that the diffusion coefficient of gold atoms is small at cryogenic temperatures [22,29].

4. Conclusions

In this study, we numerically demonstrated a PiFM measurement for single molecules on an atomic scale. By analyzing the simplified six-membered ring molecular model, we clarified the excitation conditions. We obtained PiFM images at an atomic-scale resolution, corresponding to the molecular transition states including optically allowed and forbidden transitions beyond the long-wavelength approximation. We interpreted PiFM images of single molecules in terms of the microscopic interaction between the molecular internal polarization structures and localized plasmons. In contrast, the local structure of the excited state of a single molecule can be determined from the PiFM image based on the above-type of analysis. We have also discussed the feasibility of atomic resolution measurement by PiFM. The calculated results indicate that the enhancement and localization of the electric field near the atomic-scale structure, picocavity, allows for PiFM measurements at the atomic resolution.

It is important to clarify the optical response of the local polarization structure of single molecules at the atomic resolution for the elucidation of molecular chemical reactions, development of functional metamaterials, and kinetic manipulation of molecules. PiFM is advantageous because multiple information of the localized near-field can be obtained without propagation loss, unlike other photo-assisted scanning microscopic techniques. Furthermore, it has been reported that PiFM can detect the longitudinal polarization of local chiral fields induced by chiral nanomaterials [30], which cannot be detected by SNOM [31]. PiFM measurements at the atomic resolution can allow the detection of single-molecular chirality through the near field. This will be a new capability that will outperform other types of photo-assisted scanning microscopies.

Author Contributions: Conceptualization, H.Y., N.Y. and H.I.; methodology, H.Y., N.Y. and H.I.; investigation, H.Y., N.Y. and H.I.; writing—original draft preparation, H.Y. and H.I.; writing—review and editing, H.Y., N.Y. and H.I.; supervision, H.I.; project administration, H.I.; funding acquisition, H.I. All authors read and agreed to the published version of the manuscript.

Funding: This research was funded by JSPS KAKENHI, Grant Number JP16H06504, for Scientific Research on Innovative Areas “Nano-Material Optical-Manipulation”.

Institutional Review Board Statement: Not applicable.

Informed Consent Statement: Not applicable.

Data Availability Statement: Not applicable.

Acknowledgments: The authors thank Y. Sugawara and J. Yamanishi for their fruitful discussions.

Conflicts of Interest: The authors declare no conflicts of interest.

References

1. Papakostas, A.; Potts, A.; Bagnall, D.; Prosvirnin, S.; Coles, H.; Zheludev, N. Optical manifestations of planar chirality. *Phys. Rev. Lett.* **2003**, *90*, 107404. [[CrossRef](#)] [[PubMed](#)]
2. Vallius, T.; Jefimovs, K.; Turunen, J.; Vahimaa, P.; Svirko, Y. Optical activity in subwavelength-period arrays of chiral metallic particles. *Appl. Phys. Lett.* **2003**, *83*, 234–236. [[CrossRef](#)]
3. Kuwata-Gonokami, M.; Saito, N.; Ino, Y.; Kauranen, M.; Jefimovs, K.; Vallius, T.; Turunen, J.; Svirko, Y. Giant optical activity in quasi-two-dimensional planar nanostructures. *Phys. Rev. Lett.* **2005**, *95*, 227401. [[CrossRef](#)] [[PubMed](#)]
4. Bai, B.; Svirko, Y.; Turunen, J.; Vallius, T. Optical activity in planar chiral metamaterials: Theoretical study. *Phys. Rev. A* **2007**, *76*, 023811. [[CrossRef](#)]
5. Hendry, E.; Carpy, T.; Johnston, J.; Popland, M.; Mikhaylovskiy, R.; Laphorn, A.; Kelly, S.; Barron, L.; Gadegaard, N.; Kadodwala, M. Ultrasensitive detection and characterization of biomolecules using superchiral fields. *Nat. Nanotech.* **2010**, *5*, 783. [[CrossRef](#)]
6. Kuzzyk, A.; Schreiber, R.; Fan, Z.; Pardatscher, G.; Roller, E.M.; Högele, A.; Simmel, F.C.; Govorov, A.O.; Liedl, T. DNA-based self-assembly of chiral plasmonic nanostructures with tailored optical response. *Nature* **2012**, *483*, 311. [[CrossRef](#)]
7. Kumar, J.; Eraña, H.; López-Martínez, E.; Claes, N.; Martín, V.F.; Solís, D.M.; Bals, S.; Cortajarena, A.L.; Castilla, J.; Liz-Marzán, L.M. Detection of amyloid fibrils in Parkinson's disease using plasmonic chirality. *Proc. Natl. Acad. Sci. USA* **2018**, *115*, 3225–3230. [[CrossRef](#)]
8. Mohammadi, E.; Tsakmakidis, K.L.; Askarpour, A.N.; Dehkoda, P.; Tavakoli, A.; Altug, H. Nanophotonic Platforms for Enhanced Chiral Sensing. *ACS Photon.* **2018**, *5*, 2669–2675. [[CrossRef](#)]
9. Rajapaksa, I.; Uenal, K.; Wickramasinghe, H.K. Image force microscopy of molecular resonance: A microscope principle. *Appl. Phys. Lett.* **2010**, *97*, 073121. [[CrossRef](#)]
10. Rajapaksa, I.; Kumar Wickramasinghe, H. Raman spectroscopy and microscopy based on mechanical force detection. *Appl. Phys. Lett.* **2011**, *99*, 161103. [[CrossRef](#)]
11. Imada, H.; Miwa, K.; Imai-Imada, M.; Kawahara, S.; Kimura, K.; Kim, Y. Real-space investigation of energy transfer in heterogeneous molecular dimers. *Nature* **2016**, *538*, 364–367. [[CrossRef](#)] [[PubMed](#)]
12. Imada, H.; Miwa, K.; Imai-Imada, M.; Kawahara, S.; Kimura, K.; Kim, Y. Single-molecule investigation of energy dynamics in a coupled plasmon-exciton system. *Phys. Rev. Lett.* **2017**, *119*, 013901. [[CrossRef](#)]
13. Zhang, Y.; Luo, Y.; Zhang, Y.; Yu, Y.J.; Kuang, Y.M.; Zhang, L.; Meng, Q.S.; Luo, Y.; Yang, J.L.; Dong, Z.C.; et al. Visualizing coherent intermolecular dipole–dipole coupling in real space. *Nature* **2016**, *531*, 623–627. [[CrossRef](#)] [[PubMed](#)]
14. Liu, P.; Chulhai, D.V.; Jensen, L. Single-molecule imaging using atomistic near-field tip-enhanced Raman spectroscopy. *ACS Nano* **2017**, *11*, 5094–5102. [[CrossRef](#)] [[PubMed](#)]
15. Gross, L.; Mohn, F.; Moll, N.; Liljeroth, P.; Meyer, G. The chemical structure of a molecule resolved by atomic force microscopy. *Science* **2009**, *325*, 1110–1114. [[CrossRef](#)]
16. Almajhadi, M.; Wickramasinghe, H.K. Contrast and imaging performance in photo induced force microscopy. *Opt. Express* **2017**, *25*, 26923–26938. [[CrossRef](#)]
17. Rajaei, M.; Almajhadi, M.A.; Zeng, J.; Wickramasinghe, H.K. Near-field nanoprobng using Si tip-Au nanoparticle photoinduced force microscopy with 120: 1 signal-to-noise ratio, sub-6-nm resolution. *Opt. Express* **2018**, *26*, 26365–26376. [[CrossRef](#)]
18. Yamane, H.; Yamanishi, J.; Yokoshi, N.; Sugawara, Y.; Ishihara, H. Theoretical analysis of optically selective imaging in photoinduced force microscopy. *Opt. Express* **2020**, *28*, 34787–34803. [[CrossRef](#)]
19. Yamanishi, J.; Yamane, H.; Naitoh, Y.; Li, Y.; Yokoshi, N.; Masuoka, K.; Kameyama, T.; Torimoto, T.; Ishihara, H.; Sugawara, Y. Optical Force Mapping at the Single-Nanometre Scale. *Nat. Commun.* **2021**, *12*, 3865. [[CrossRef](#)]
20. Yamanishi, J.; Naitoh, Y.; Li, Y.; Sugawara, Y. Heterodyne technique in photoinduced force microscopy with photothermal effect. *Appl. Phys. Lett.* **2017**, *110*, 123102. [[CrossRef](#)]
21. Yamanishi, J.; Naitoh, Y.; Li, Y.; Sugawara, Y. Heterodyne Frequency Modulation in Photoinduced Force Microscopy. *Phys. Rev. Appl.* **2018**, *9*, 024031. [[CrossRef](#)]
22. Benz, F.; Schmidt, M.K.; Dreismann, A.; Chikkaraddy, R.; Zhang, Y.; Demetriadou, A.; Carnegie, C.; Ohadi, H.; De Nijs, B.; Esteban, R.; et al. Single-molecule optomechanics in “picocavities”. *Science* **2016**, *354*, 726–729. [[CrossRef](#)] [[PubMed](#)]
23. Takase, M.; Ajiki, H.; Mizumoto, Y.; Komeda, K.; Nara, M.; Nabika, H.; Yasuda, S.; Ishihara, H.; Murakoshi, K. Selection-rule breakdown in plasmon-induced electronic excitation of an isolated single-walled carbon nanotube. *Nat. Photonics* **2013**, *7*, 550. [[CrossRef](#)]
24. Iida, T.; Ishihara, H. Theory of resonant radiation force exerted on nanostructures by optical excitation of their quantum states: From microscopic to macroscopic descriptions. *Phys. Rev. B* **2008**, *77*, 245319. [[CrossRef](#)]
25. Johnson, P.B.; Christy, R.W. Optical constants of the noble metals. *Phys. Rev. B* **1972**, *6*, 4370. [[CrossRef](#)]
26. Antoine, R.; Brevet, P.F.; Girault, H.H.; Bethell, D.; Schiffrin, D.J. Surface plasmon enhanced non-linear optical response of gold nanoparticles at the air/toluene interface. *Chem. Commun.* **1997**, 1901–1902. [[CrossRef](#)]
27. Tsuda, A.; Osuka, A. Fully conjugated porphyrin tapes with electronic absorption bands that reach into infrared. *Science* **2001**, *293*, 79–82. [[CrossRef](#)]
28. Mukai, K.; Abe, S. Effects of positional disorder on optical absorption spectra of light-harvesting antenna complexes in photosynthetic bacteria. *Chem. Phys. Lett.* **2001**, *336*, 445–450. [[CrossRef](#)]

29. Carnegie, C.; Griffiths, J.; de Nijs, B.; Readman, C.; Chikkaraddy, R.; Deacon, W.M.; Zhang, Y.; Szabó, I.; Rosta, E.; Aizpurua, J.; et al. Room-temperature optical picocavities below 1 nm³ accessing single-atom geometries. *J. Phys. Chem. Lett.* **2018**, *9*, 7146–7151. [[CrossRef](#)] [[PubMed](#)]
30. Ishihara, H.; Hoshina, M.; Yamane, H.; Yokoshi, N. Light-Nanomatter Chiral Interaction in Optical-Force Effects. In *Chirality, Magnetism and Magnetoelectricity: Separate Phenomena and Joint Effects in Metamaterial Structures*; Kamenetskii, E., Ed.; Springer: Cham, Switzerland, 2021; Chapter 5, pp. 105–126.
31. Hashiyada, S.; Narushima, T.; Okamoto, H. Imaging chirality of optical fields near achiral metal nanostructures excited with linearly polarized light. *ACS Photonics* **2018**, *5*, 1486–1492. [[CrossRef](#)]